This is a preprint, the final version is subject to change, of the American Mineralogist (MSA)
Cite as Authors (Year) Title. American Mineralogist, in press.
(DOI will not work until issue is live.) DOI: http://dx.doi.org/10.2138/am-2017-5830

Ab initio study of the structure and stability of $CaMg(CO_3)_2$ at high pressure - Revision 1

Natalia V. Solomatova and Paul D. Asimow

Division of Geological & Planetary Sciences, Caltech, Pasadena, CA 91125 U.S.A.

Abstract

Dolomite is one of the major mineral forms in which carbon is subducted into the Earth's mantle. End-member $CaMg(CO_3)_2$ dolomite typically breaks down upon compression into two carbonates at 5-6 GPa in the temperature range of 800-1200 K (Shirasaka et al. 2002). However, high-pressure X-ray diffraction experiments have shown that dense high-pressure polymorphs of dolomite may be favored over single-cation carbonates (Santillan et al. 2003; Mao et al. 2011; Merlini et al. 2012). Here we compare calculated dolomite structures to experimentally observed phases. Using density functional theory interfaced with a genetic algorithm that predicts crystal structures (USPEX), a monoclinic phase with space group *C2/c* was found to have lower energy at pressures above 15 GPa than all previously reported dolomite structures. It is possible that this phase is not observed experimentally due to a large activation energy of transition from dolomite I, resulting in the observed second-order phase transition to a metastable dolomite II. Due to the complex energy landscape for candidate high-pressure dolomite structures, a number of structurally unique metastable polymorphs exist. We calculate the equation of state of a set of lowest-energy dolomite polymorphs with space groups *P-1*, *P2/c* and *C2/c* up to 80 GPa. Our results demonstrate a need for calculations and experiments on Fe-Mn bearing high-pressure carbonate phases to extend our understanding of Earth's deep carbon cycle and test whether high-pressure polymorphs of double-cation carbonates represent the main reservoir for carbon storage within downwelling regions of Earth's mantle.

Keywords: dolomite, ab initio, global carbon cycle, lower mantle, high pressure

Introduction

Carbon is exchanged between the surface and Earth's interior through ingassing by subduction and through both passive and volcanic outgassing (Kelemen and Manning 2015). Carbon is subducted into the mantle primarily in the form of carbonate (CO_3^{2-}-bearing) minerals as metasomatically calcium-enriched basaltic rock (rodingite), calcified serpentinites (ophicarbonates) and sedimentary carbonaceous ooze (Brenker et al. 2006). Evidence of carbon-bearing phases in the Earth's mantle includes: the release of CO_2 in volcanic eruptions, dissolved CO_2 in magmatic glasses and glass inclusions (Mörner and Etiope 2002), diamonds and carbonate minerals in mantle xenoliths (Eggler 1978; Sobolev and Shatsky, 1990), and the existence of carbonatite and kimberlite magmas (Wyllie et al. 1990). Carbon has low solubility in mantle silicates (Shcheka et al. 2006), such that significant carbon storage or transport in the mantle requires formation of carbon-rich phases. Decomposition of carbonates can produce free CO_2, which lowers the viscosity and melting temperature of the surrounding mantle (Eggler et al. 1976) and enables rapid recycling of carbon through subduction-related volcanism rather than deep subduction and long-term storage. Identifying and characterizing the stability of carbonate phases is therefore a necessary step towards understanding the transport and storage of carbon through the Earth's deep carbon cycle (Hazen et al., 2013). The identification of a new, more stable carbonate phase that is able to host carbon under conditions where known carbonates may decompose has the potential to substantially change estimates of the geochemical fluxes of carbon.

It has been suggested that magnesite is the dominant carbonate phase in relatively oxidized regions of the mantle (Brenker et al. 2006; Isshiki et al. 2004). Skorodumova et al. (2005), reasoning by analogy to silicates, examined the stability of magnesite in selected pyroxene and perovskite structures, finding that magnesite could transform into a *C2/c* pyroxene structure with 4-fold coordination of carbon by oxygen at 113 GPa. Using USPEX, however, Oganov et al. (2008) searched a vastly larger space of possible structures and found that magnesite undergoes a phase transition at 84 GPa to a monoclinic phase ("phase II") with space group *C2/m,* containing rings of $(C_3O_9)^{6-}$, and subsequently at 138 GPa transitions to an orthorhombic phase ("phase III") with space group $P2_1$, containing chains of CO_4^{4-} tetrahedra. Their calculations show that the *C2/c* pyroxene structure has a higher energy than either phase II or phase III at all relevant pressures. Calcite, on the other hand, transitions to aragonite at 2 GPa, which transitions to the post-aragonite phase (space group *Pmmn*) at 42 GPa, persisting up to core-mantle boundary pressures (Ono et al. 2005; Oganov et al. 2006).

End-member $CaMg(CO_3)_2$ dolomite typically breaks down into two carbonates at about 5-6 GPa in the temperature range of 800-1200 K (Shirasaka et al. 2002). However, X-ray diffraction experiments have proposed that dense high-pressure phases of dolomite may be more stable or comparable in stability to single-cation carbonates above 35 GPa. High-pressure dolomite may be resistant to decomposition into single-cation carbonates prior to the transformation of trigonal magnesite to monoclinic phase II. Santillan et al. (2003) observed a phase transition of $CaMg(CO_3)_2$ dolomite to a new phase ("dolomite II") at about 20 GPa. Experiments on two Fe-bearing compositions, $Ca_{0.988}Mg_{0.918}Fe_{0.078}Mn_{0.016}(CO_3)_2$ (Mao et al. 2011) and $CaMg_{0.6}Fe_{0.4}(CO_3)_2$ (Merlini et al. 2012), led to observations of two phase transitions in dolomite at 17 and 35 GPa. Both studies refer to the high-pressure phases as "dolomite II" and

"dolomite III," and find that dolomite II decomposes upon heating while dolomite III is resistant to decomposition into single-cation carbonates at high pressure and temperature. However, they report different high-pressure dolomite phases. Mao et al. (2011) characterize their observed dolomite II with orthorhombic symmetry and dolomite III with monoclinic symmetry, but did not refine atomic coordinates or identify the space groups. Merlini et al. (2012) characterize their high-pressure dolomite phases with triclinic symmetry, refining both the crystal structures and atomic coordinates. The X-ray diffraction patterns for the dolomite II structures are consistent with each other (see supplementary materials for Merlini et al. (2012)), whereas the dolomite III structures have distinct X-ray diffraction patterns resulting from nonequivalent crystal structures. The difference in symmetry reflects the complex nature of dolomite polymorphs, whose stability and transformation kinetics may be strongly affected by variations in composition and experimental conditions. As already seen in comprehensive structure searches for $MgCO_3$, it is likely that Fe-Mn-bearing $CaMg(CO_3)_2$ has a complex energy landscape, resulting in many polymorphs with similar energies. Even after sample annealing, it may be that the most stable phase is never achieved experimentally or that slight variations in composition result in different ground states.

In addition to a difference in symmetry, the two studies report different unit-cell volumes for dolomite II and dolomite III, with discrepancies larger than can be explained simply by the difference in composition. Mao et al. (2011) report a 15% unit-cell volume drop upon the phase transition from dolomite I to dolomite II, whereas Merlini et al. (2012) do not observe a detectable change in volume. For the phase transition from dolomite II to dolomite III, Mao et al. (2011) report an 8% volume drop and Merlini et al. (2012) report a 3% volume drop. Although it is possible that the difference in unit cell volumes for the high pressure phases is a result of the

combined effect of different compositions, crystal structures and experimental conditions, Merlini et al. (2012) propose that a different choice of formula units per unit cell is required to correctly index the structure of Mao et al. (2011). In any case, the differing experimental observations create a need for a theoretical study to confirm which high-pressure dolomite phases are the most thermodynamically stable.

Computational Methods

USPEX (Universal Structure Predictor: Evolutionary Xtallography), an evolutionary algorithm that can be interfaced with a variety of density functional theory codes, has been shown to successfully predict stable phases without experimental input (Oganov and Glass, 2006). USPEX compares the energies of structures that continuously evolve through operations of (1) heredity – a combination of two parent structures, (2) lattice mutations – a distortion of the cell shape through a symmetric strain matrix, and (3) atomic permutations – switching of atoms within the cell. We ran USPEX interfaced with the ab initio code VASP (Kresse and Furthmuller 1996) for $CaMg(CO_3)_2$ with 20 or 30 atoms/cell at 25-40 GPa pressure, with population sizes between 30 and 50 structures per generation. Ab initio calculations were performed at 0 K using the projector-augmented wave (PAW) method (Blochl, 1994) implemented in VASP. The generalized gradient approximation (GGA) (Perdew et al. 1996) was used to approximate the exchange correlation terms. In structure prediction calculations, GGA produces results better than LDA in terms of agreement with experiments for phase transition pressures and chemical reactions (Oganov et al. 2013). The following PAW pseudo-potentials were used in VASP for structure prediction: core radius of 3.7 a.u. for Ca ($1s^2 2s^2 2p^6$ core, $3s^2 3p^6 4s^2$ valence), 2.0 a.u. for Mg ($1s^2 2s^2 2p^6$ core, $3s^2$ valence), 1.5 a.u. for C ($1s^2$ core, $2s^2 2p^2$ valence), and 1.52 a.u. for O ($1s^2$ core, $2s^2 2p^4$ valence).

These calculations were run several times both with and without prescribed seed structures. The first generation was created either entirely randomly or with 1-3 seeded structures with standard physical constraints on the minimum ion distance of 0.7 Å and minimum lattice vector of 2-2.5 Å. For subsequent generations, 40-50% of the structures were created through heredity using the lowest energy structures from the previous generation, 10-20% were produced through lattice mutations, 10% were produced through atomic permutations and 20% were randomly generated. The best five structures in each generation were left unchanged and competed in subsequent generations. Generated structures were relaxed at constant pressure in four stages with incrementally increasing precision, where the final plane-wave energy cut off, k-point resolution and convergence criteria for electronic self-consistency were 550 eV, 0.08 $Å^{-1}$ and 10^{-5} eV, respectively. Through this procedure, we were able to find a 20-atom monoclinic dolomite with *P2/c* symmetry and a 20-atom primitive *C2/c* cell to which we applied a crystallographic transformation matrix to obtain the conventional 40-atom monoclinic *C2/c* structure. Due to the complex nature of the free energy landscape for double carbonates, it is possible that a global minimum was never achieved.

A *C2/c* structure with 4-fold C was created by substituting the dolomitic composition into the diopside structure and relaxing it at high pressure. We also examined the triclinic dolomite II and dolomite III structures from Merlini et al. (2012), and we substituted the dolomitic composition into several previously published carbonate structures: the post-aragonite structure (*Pmmn*) (Oganov et al. 2006); $MgCO_3$ phase II (*C2/m*), phase III ($P2_1$), structure $P2_1$-10 and structure $Pna2_1$-20 (Oganov et al. 2008); calcite III (*C2*) (Smyth and Ahrens 1997); and $MnCO_3$ phase II (*P-1*) (Merlini et al. 2015). Appropriate supercells with the dolomite stoichiometry were created with various choices of cation site ordering (i.e., layers of Ca/Mg atoms and checkered

Ca/Mg arrangement). The $P2_1$-10 structure has the space group *C2* after relaxing it at high pressures with the dolomite stoichiometry. The resulting structure was crystallographically transformed to a conventional *C2* unit cell, and resembles the *P2/c* structure. The relaxed calcite III structure extended to a 1x1x2 supercell with layers of Ca and Mg atoms is equivalent to the *C2* structure with a different unit cell. These structures from the literature and several competitive structures found with USPEX are not considered further in this study due to their relatively high energies. However, it is possible that, with certain cation substitutions, these phases may be observed experimentally. Hence, all of these structures are provided in the supplementary crystallographic information file.

Finally, the short list of low-energy candidate dolomite structures remaining after USPEX and literature search were relaxed using more accurate PAW pseudo-potentials for the 3rd-row elements: core radius of 2.3 a.u. for Ca ($1s^2 2s^2 2p^6$ core, $3s^2 3p^6 4s^2$ valence) and 2.0 a.u. for Mg ($1s^2 2s^2$ core, $2p^6 3s^2$ valence). C and O pseudo-potentials remained the same. A plane-wave energy cut off of 600 eV was used and a fine k-point grid of 0.02-0.03 $Å^{-1}$ was required to refine the transition pressures between phases with similar energies. We carried out all the requisite convergence tests to ensure these parameters were adequate. The convergence criteria for electronic self-consistency and ionic relaxation loop are 10^{-5} eV and 10^{-4} eV, respectively. We ensured that forces acting on all relaxed atoms were <0.01 eV/Å.

The pressure-volume data were fitted with third-order Birch-Murnaghan equations of state using MINUTI 1.1.2 (Sturhahn 2015). For dolomite III and *P2/c* dolomite, equations of states were fitted above 10 GPa; at lower pressures, these structures transform into lower-pressure polymorphs with coplanar CO_3^{2-} groups during structural relaxation. Similarly, in *C2/c* dolomite with 4-fold C, the carbonate tetrahedra transform to triangular coordination

159 environments below 60 GPa. Thus, for the *C2/c* structure with 4-fold C, equation of state
160 parameters V_0, K_0 and K_0', though defined at 0 pressure, are fitted to data in the range from 60 to
161 140 GPa. Conversely, the dolomite II structure is not stable above 30 GPa; thus, an equation of
162 state was fitted to the pressure range between 0 and 30 GPa. Structures *C2/c* with 3-fold C and
163 dolomite I were fitted with equations of state at pressures between 0 and 80 GPa.

164 **Results**

165 We found two competitive $CaMg(CO_3)_2$ structures with *C2/c* and *P2/c* symmetry using
166 USPEX (Fig. 1). Simulated X-ray diffraction patterns are shown in Figure 2. The enthalpy
167 difference between candidate high-pressure dolomite polymorphs and *R-3* dolomite I are shown
168 in Figure 3. For static ab initio calculations, the enthalpy is equivalent to Gibbs free energy; the
169 structure with the lowest enthalpy is the most stable structure. Dolomite II is energetically
170 similar to dolomite I and was not successfully relaxed above 30 GPa without the rotation of its
171 CO_3 groups (i.e., a second order phase transition). The *P2/c* structure is less stable than the *C2/c*
172 structure at all pressures examined in this study but more stable than the dolomite III structure
173 above 32 GPa. Above 15 GPa, the *C2/c* structure is more favorable than all other structures
174 discovered by USPEX in this study and all previously reported structures. There is a shift from
175 sp^2 bonding (triangular coordination) to sp^3 bonding (tetrahedral coordination) in the *C2/c*
176 structure at 127.5 GPa (Fig. 3 inset).

177 The pressure-volume relationship for the candidate dolomite phases and their
178 corresponding third-order Birch-Murnaghan equations of state (EOS) are shown in Figure 4. The
179 zero-pressure volume per CO_3^{2-} group (V_0), bulk modulus (K_0) and the bulk modulus derivative
180 (K'_0) for these structures are compared in Table 2. The fitted K_0 and K_0' for dolomite I are

86.8(3) GPa and 4.20(2) with a V_0 of 55.1 $Å^3$, in reasonable agreement with reported equation of state parameters determined from fitting a Birch-Murnaghan EOS to pressure-volume data from X-ray diffraction experiments: V_0=53.4(1) $Å^3$, K_0=94.1(7) with a fixed K_0' of 4 (Ross and Reeder 1992). The volume of dolomite I is overestimated by 3.3%, which is typical for the GGA method. We fitted the experimental pressure-volume data for $Ca(Mg_{0.6}Fe_{0.4})(CO_3)_2$ dolomite III (Merlini et al. 2012) with a third-order Birch Murnaghan EOS using a prior estimate of 4 and prior window of ±1 for K_0', resulting in V_0=51.8(1.6) $Å^3$, K_0=92.7(20.0) GPa and K_0'=3.92(4). These results are in good agreement with the equation of state parameters fitted to the calculated dolomite III compression data where V_0=52.2(1) $Å^3$, K_0=94.1(9) GPa and K_0'=3.89(3).

For high-spin $Ca(Mg_{0.92}Fe_{0.08})(CO_3)_2$ dolomite III, Mao et al. (2008) report a K_0=164(4) with a K_0'=4 (fixed), resembling the compression behavior of our calculated *C2/c* dolomite with 4-fold coordination. The zero-pressure bulk moduli for all phases with triangular $(CO_3)^{2-}$ groups range from 80 to 90 GPa, whereas the K_0 for the *C2/c* structure with 4-fold C is 180 GPa, more than twice as large as for the *C2/c* structure with 3-fold C. By 80 GPa, however, the difference in bulk moduli decreases to 30 GPa (Fig. 4 inset). Nevertheless, a high bulk modulus for high-pressure carbonates may be an indication of 4-fold coordinated C.

Discussion

In mantle silicates, Si changes from 4-fold to 6-fold coordination at the decomposition of ringwoodite to bridgmanite and periclase. In $MgCO_3$, C forms tetrahedra above 82 GPa, whereas in $CaCO_3$, C remains 3-fold coordinated up to core-mantle boundary pressures, only forming tetrahedra above 137 GPa (Oganov et al. 2008; Boulard et al., 2015). In *C2/c* dolomite, C tetrahedra become stable at 127.5 GPa, an intermediate pressure compared to the tetrahedra-

forming pressures for the single-carbonate end members, $MgCO_3$ and $CaCO_3$. Prior to these calculations, there have been no reports in the literature addressing whether C in double carbonates, such as dolomite, would become tetrahedrally coordinated at lower mantle pressures.

With increasing pressure, Mg, Fe^{2+} and Ca in mantle silicates transition from 6-fold coordination in olivine and pyroxenes to 6- and 8-fold coordination in garnets and then to 6- and 12-fold coordination in bridgmanite (Murakami et al. 2004; Oganov and Ono 2004). In $CaCO_3$, Ca increases in coordination number from 6 in calcite to 9 in aragonite to 12 in post-aragonite while, in $MgCO_3$, Mg atoms increase in coordination from 6 in magnesite to 8-10 in phases II and III to 9 in *Pna2₁*-20 (Oganov et al. 2008). In the dolomite III structure (Merlini et al. 2012), the coordination numbers are variable, ranging from 7 to 10, with Ca occupying the larger sites. In *C2/c* dolomite, Mg is 6-fold coordinated and Ca is 8-fold coordinated up to at least 140 GPa. Although, at high pressure, *C2/c* dolomite is the least dense $CaMg(CO_3)_2$ candidate, it is stiffer than all the other considered phases in this study, a result of the persistence of relatively low coordination values for its metal cations.

Our simulations show that dolomite has many energetically competitive polymorphs at high pressure with similar enthalpies to the *P2/c* and dolomite III structures; however, above 15 GPa, the *C2/c* structure with 3-fold C has a lower energy than all other phases found with USPEX and reported structures in literature. It is possible that the *C2/c* structure has not been observed experimentally due to a high activation barrier and/or a high sensitivity of the crystal symmetry to iron concentration. Additionally, it is very likely that the stability of high-pressure dolomite with respect to decomposition into single-cation carbonates is related to its composition.

Pure high-pressure dolomite phases will likely decompose into single-cation carbonates at high pressures. The rapid decrease of the enthalpy of high-density post-aragonite beyond 42 GPa is the main driver of the predicted breakdown of all dolomites into single-cation carbonates, including the most stable *C2/c* polymorph (Fig. 5). However, the addition of Fe and Mn is likely to stabilize dolomite with respect to decomposition. A careful treatment of iron is necessary to accurately describe the strongly correlated nature of the *d*-electrons using self-consistently calculated Hubbard *U* parameters, which are a function of iron concentration, spin state, crystal symmetry and unit-cell volume. Additionally, the effect of temperature on high-pressure dolomite phases is unknown. The stability field of pure dolomite I increases with increasing temperature, decomposing at about 4 GPa at 400 K and 6 GPa at 1200 K (Martinez et al. 1996). It is possible that a similar trend is true for high-pressure dolomite polymorphs. Additional calculations and experiments on Fe-bearing dolomites at high temperatures and pressures are needed.

Implications

The behavior of high-pressure carbonates influences the global carbon cycle and, subsequently, global climate over geologic time scales. The feedbacks inherent in the formation and destruction of carbonate and the role of carbonate in storage of the potent greenhouse gas CO_2 are central to maintaining the habitability of our planet. It has been suggested that Ca-Mg-Fe carbonates play a leading role in transporting and storing carbon in the deep earth (Brenker et al. 2007; Boulard et al. 2012). Although the present study of pure $CaMg(CO_3)_2$ dolomite has identified new, more stable high pressure phases than those previously known, it has not yet changed our understanding of the ultimate stability of double carbonates relative to their decomposition products. However, when Fe is considered in future calculations, we may find

that high-pressure polymorphs of Fe-bearing dolomite could in fact represent the main reservoir for carbon storage within sections of the Earth's mantle. Combined with thermodynamic, geochemical and tectonic models, these results will help us understand the effect of the global carbon cycle on long-term climate change.

Acknowledgments

We would like to thank Edwin Schauble, Abby Kavner, Marco Merlini, Greg Finkelstein, Artem Oganov and Olle Hellman for valuable discussions and insights. We are thankful to Naveed Near-Ansari for assistance with technical aspects using FRAM, the high-performance computing cluster at Caltech. This work is supported by the US National Science Foundation through award EAR-1551433.

References Cited

Blöchl, P.E. (1994) Projector augmented-wave method. Physical Review B, 50, 17953.

Boulard, E., Menguy, N., Auzende, A.L., Benzerara, K., Bureau, H., Antonangeli, D., Corgne, A., Morard, G., Siebert, J., Perrillat, J.P. and Guyot, F. (2012) Experimental investigation of the stability of Fe-rich carbonates in the lower mantle. Journal of Geophysical Research: Solid Earth, 117.

Boulard, E., Pan, D., Galli, G., Liu, Z., and Mao, W.L. (2015) Tetrahedrally coordinated carbonates in Earth's lower mantle. Nature communications, 6.

Brenker, F.E., Vollmer, C., Vincze, L., Vekemans, B., Szymanski, A., Janssens, K., and Kaminsky, F. (2006) CO_2-recycling to the deep convecting mantle. Geochimica et Cosmochimica Acta, 70, A66.

Brenker, F.E., Vollmer, C., Vincze, L., Vekemans, B., Szymanski, A., Janssens, K., Szaloki, I., Nasdala, L., Joswig, W., and Kaminsky, F. (2007) Carbonates from the lower part of transition zone or even the lower mantle. Earth and Planetary Science Letters, 260, 1-9.

Eggler, D.H. (1976) Does CO_2 cause partial melting in the low-velocity layer of the mantle? Geology, 4, 69-72.

Eggler, D.H. (1987) Solubility of major and trace elements in mantle metasomatic fluids: experimental constraints. Mantle Metasomatism , Academic Press London, 21-41.

Hazen, R.M., Jones, A.P. and Baross, J.A. (eds) (2013) Carbon in Earth. Mineralogical Society of America and Geochemical Society, Reviews in Mineralogy and Geochemistry 75.

Isshiki, M., Irifune, T., Hirose, K., Ono, S., Ohishi, Y., Watanuki, T., Nishibori, E., Takata, M., and Sakata, M. (2004) Stability of magnesite and its high-pressure form in the lowermost mantle. Nature 427, 60-63.

Kelemen, P.B., and Manning, C.E. (2015) Reevaluating carbon fluxes in subduction zones, what goes down, mostly comes up. Proceedings of the National Academy of Sciences 112, E3997-E4006.

Kresse, G., and Furthmüller, J. (1996) Efficiency of *ab-initio* total energy calculations for metals and semiconductors using a plane-wave basis set. Computational Materials Science, 6(1), 15-50.

Mao, Z., Armentrout, M., Rainey, E., Manning, C.E., Dera, P., Prakapenka, V.B., and Kavner, A. (2011) Dolomite III: A new candidate lower mantle carbonate. Geophysical Research Letters, 38.

290 Martinez, I., Zhang, J., and Reeder, R. J. (1996) In situ X-ray diffraction of aragonite and
291 dolomite at high pressure and high temperature; evidence for dolomite breakdown to
292 aragonite and magnesite. American Mineralogist, 81, 611-624.

293 Merlini, M., Crichton, W.A., Hanfland, M., Gemmi, M., Müller, H., Kupenko, I., and
294 Dubrovinsky, L. (2012) Structures of dolomite at ultrahigh pressure and their influence
295 on the deep carbon cycle. Proceedings of the National Academy of Sciences, 109, 13509-
296 13514.

297 Momma, K. and Izumi, F. (2008) VESTA: a three-dimensional visualization system for
298 electronic and structural analysis, Journal of Applied Crystallography, 41, 653-658.

299 Mörner, N.A., and Etiope, G. (2002) Carbon degassing from the lithosphere. Global and
300 Planetary Change, 33, 185-203.

301 Murakami, M., Hirose, K., Kawamura, K., Sata, N. and Ohishi, Y. (2004) Post-perovskite phase
302 transition in $MgSiO_3$. Science, 304, 855-858.

303 Oganov, A.R., and Ono, S. (2004) Theoretical and experimental evidence for a post-perovskite
304 phase of $MgSiO_3$ in Earth's D″ layer. Nature, 430, 445-448.

305 Oganov, A.R., and Glass, C.W. (2006) Crystal structure prediction using ab initio evolutionary
306 techniques: Principles and applications. The Journal of chemical physics, 124, 244704.

307 Oganov, A.R., Glass, C.W., and Ono, S. (2006) High-pressure phases of $CaCO_3$: crystal structure
308 prediction and experiment. Earth and Planetary Science Letters, 241, 95-103.

Oganov, A.R., Ono, S., Ma, Y., Glass, C.W., and Garcia, A. (2008) Novel high-pressure structures of $MgCO_3$, $CaCO_3$ and CO_2 and their role in Earth's lower mantle. Earth and Planetary Science Letters, 273, 38-47.

Oganov, A.R., Hemley, R.J., Hazen, R.M. and Jones, A.P. (2013) Structure, bonding, and mineralogy of carbon at extreme conditions. Reviews in Mineralogy and Geochemistry, 75, 47-77.

Ono, S., Kikegawa, T., Ohishi, Y., and Tsuchiya, J. (2005) Post-aragonite phase transformation in $CaCO_3$ at 40 GPa. American Mineralogist, 90, 667-671.

Perdew, J.P., Burke, K. and Ernzerhof, M. (1996) Generalized gradient approximation made simple. Physical review letters, 77, 3865.

Ross, N.L. and Reeder, R.J. (1992) High-pressure structural study of dolomite and ankerite. American Mineralogist, 77, 412-421.

Santillán, J., Williams, Q., and Knittle, E. (2003) Dolomite-II: A high-pressure polymorph of $CaMg(CO_3)_2$. Geophysical Research Letters, 30.

Shcheka, S.S., Wiedenbeck, M., Frost, D.J., and Keppler, H. (2006) Carbon solubility in mantle minerals. Earth and Planetary Science Letters, 245, 730-742.

Shirasaka, M., Takahashi, E., Nishihara, Y., Matsukage, K., & Kikegawa, T. (2002) In situ X-ray observation of the reaction dolomite= aragonite+ magnesite at 900–1300 K. American Mineralogist, 87, 922-930.

328 Skorodumova, N.V., Belonoshko, A.B., Huang, L., Ahuja, R., and Johansson, B. (2005) Stability
329 of the $MgCO_3$ structures under lower mantle conditions. American mineralogist, 90,
330 1008-1011.

331 Smyth, J.R., and Ahrens, T.J. (1997) The crystal structure of calcite III. Geophysical Research
332 Letters, 24, 1595-1598.

333 Sobolev, N.V., and Shatsky, V.S. (1990) Diamond inclusions in garnets from metamorphic
334 rocks: a new environment for diamond formation. Nature 343, 742-746.

335 Sturhahn, W. (2015) MINUTI open source software, version 1.1.2, www.nrixs.com.

336 Wyllie, P.J., Baker, M.B., and White, B.S. (1990) Experimental boundaries for the origin and
337 evolution of carbonatites. Lithos, 26, 3-19.

Figure Captions

Figure 1. Novel high-pressure dolomite polymorphs at 80 GPa: (a) *C2/c* dolomite with 3-fold C, (b) *C2/c* dolomite with 4-fold C and (c) *P2/c* dolomite. Figures were produced with the VESTA software (Momma and Izumi 2008). Ca polyhedra are blue, Mg polyhedra are grey and C polyhedra are orange.

Figure 2. Synthetic X-ray diffraction patterns for high-pressure dolomite phases at 80 GPa (λ=1.54 Å). Dolomite III is blue, *C2/c* dolomite with 3-fold C is red, *C2/c* dolomite with 4-fold C is grey and *P2/c* dolomite is orange.

Figure 3. Enthalpies per formula unit of candidate dolomite structures relative to dolomite I (horizontal line at zero). *C2/c* dolomite is energetically more stable than all other phases examined in this study for the $CaMg(CO_3)_2$ composition. Inset shows the enthalpy (H) per formula unit of *C2/c* dolomite 4-fold C relative to *C2/c* dolomite with 3-fold C. The transition from sp^2 bonding (triangular coordination) to sp^3 bonding (tetrahedral coordination) of C in the *C2/c* structure occurs at 127.5 GPa.

Figure 4. Pressure-volume data and the fitted third-order Birch Murnaghan equations of state for candidate dolomite phases. Experimental pressure-volume data for $CaMg_{0.6}Fe_{0.4}(CO_3)_2$ are shown in grey "+" symbols, with a second-order phase transition to dolomite II at 17 GPa and a first-order phase transition to dolomite III at 35 GPa (Merlini et al. 2012). The equation of state for *C2/c* dolomite with 4-fold C was calculated from data at 60-140 GPa in intervals of 5 GPa. Inset shows the fitted bulk modulus as a function of pressure. Structures *C2/c* and *P2/c* have indistinguishable bulk moduli.

Figure 5. The enthalpy difference between dolomite polymorphs and aragonite + magnesite. The rapid decrease of the enthalpy of the post-aragonite + magnesite assemblage is the main driver of the breakdown of all dolomites into single-cation carbonates. However, the substitution of Fe for Mg is likely to stabilize *C2/c* dolomite with respect to decomposition.

Tables

Table 1. Fractional coordinates, lattice parameters and unit-cell volume for calculated high-pressure $CaMg(CO_3)_2$ polymorphs at 80 GPa.

C2/c (3-fold C) (Z = 4) a=8.0127, b=7.6005, c=4.8652, α=90, β=106.43, γ=90, V=284.20			
atom	x	y	z
Ca	0.00000	0.67015	0.75000
Mg	0.50000	0.40958	0.25000
C	0.21854	0.36747	0.81476
O1	0.37765	0.40733	0.85578
O2	0.33535	0.73448	0.83822
O3	0.13315	0.44102	0.96001
C2/c (4-fold C) (Z = 4) a=8.3072, b=7.8089, c=4.3586, α=90, β=103.53, γ=90, V=274.89			
atom	x	y	z
Ca	0.00000	0.68472	0.75000
Mg	0.50000	0.39288	0.25000
C	0.21954	0.40787	0.76878
O1	0.37742	0.42091	0.83232
O2	0.33653	0.75551	0.80211
O3	0.14558	0.47281	0.00112
P2/c (Z = 2) a=6.4089, b= 2.8246, c=7.7595, α=90, β=92.54, γ=90, V=140.32			
atom	x	y	z
Ca	0.00000	0.19756	0.25000
Mg	0.50000	0.80172	0.25000
C	0.73864	0.56617	0.99292
O1	0.75561	0.29761	0.64840
O2	0.59086	0.71271	0.89469
O3	0.86966	0.27650	0.94243

Table 2. Equation of state parameters for the calculated $CaMg(CO_3)_2$ and experimental $Ca(Mg,Fe)(CO_3)_2$ polymorphs. We fitted the pressure-volume data using a third-order Birch-Murnaghan equation of state with the MINUTI software, applying a 1% error to pressure and volume. V_0 is the zero-pressure volume per CO_3^{2-} group. Dolomite III and structures *P2/c* and *C2/c* with 4-fold C were not successfully relaxed at 0 GPa without a second-order phase transition to a lower-pressure structure. Thus, their zero-pressure volumes were fitted.

Phase	V_0 (Å^3)	K_0 (GPa)	K_0'
dolomite I	55.1	86.8(3)	4.20(2)
dolomite II[a]	55.0	94.0(8)	2.80(7)
dolomite III[b]	52.2(1)	94.1(9)	3.89(3)
dolomite III[c] (Mao et al. 2011)	39.9(3)	164(8)	4
dolomite III[d] (Merlini et al. 2012)	51.8(1.6)	92.7(20.0)	3.92(4)
C2/c (3-fold C)	51.9	84.8(6)	4.78(5)
C2/c (4-fold C)	45.1(3)	178.4(8.1)	3.69(9)
P2/c	51.2(1)	85.4(1.4)	4.76(6)

[a] We fitted an equation of state to our calculated pressure-volume data for the triclinic dolomite II structure reported in Merlini et al. (2012).

[b] We fitted an equation of state to our calculated pressure-volume data for the triclinic dolomite III structure reported in Merlini et al. (2012).

[c] Equation of state parameters as reported in Mao et al. (2011) for their observed monoclinic dolomite III structure. K_0' was fixed to 4. The full composition as determined from microprobe analysis is $Ca_{0.988}Mg_{0.918}Fe_{0.078}Mn_{0.016}(CO_3)_2$. It is possible that the volume of dolomite III is underestimated due to an incorrect assumption of the number of formula units per unit cell (Merlini et al. 2012).

[d] We fitted an equation of state to the published experimental pressure-volume data for triclinic dolomite III, with the chemical formula $CaMg_{0.6}Fe_{0.4}(CO_3)_2$ (Merlini et al. 2012). We used a prior estimate of 4 and prior window of ±1 for K_0'.

This is a preprint, the final version is subject to change, of the American Mineralogist (MSA)
Cite as Authors (Year) Title. American Mineralogist, in press.
(DOI will not work until issue is live.) DOI: http://dx.doi.org/10.2138/am-2017-5830

Fig 1a

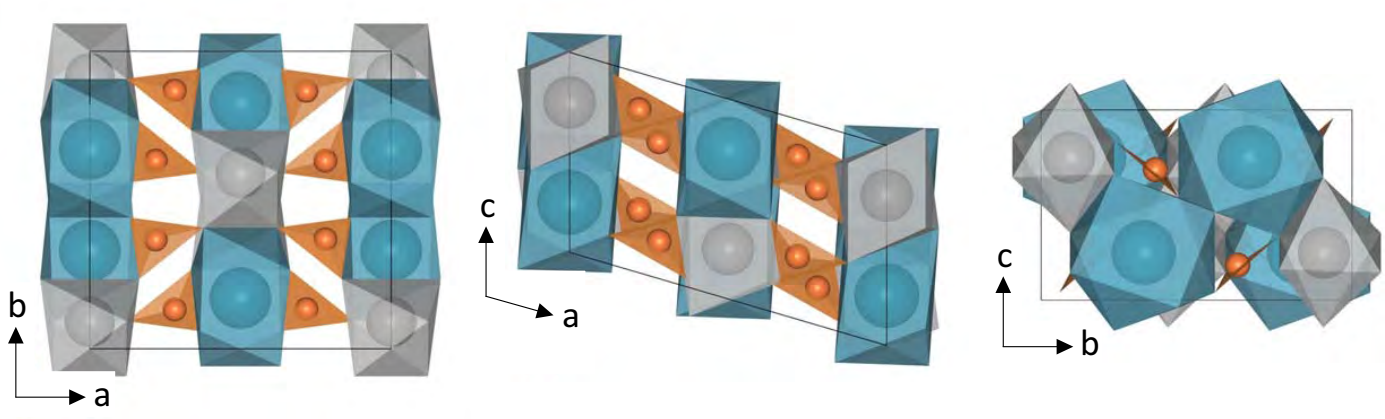

This is a preprint, the final version is subject to change, of the American Mineralogist (MSA)
Cite as Authors (Year) Title. American Mineralogist, in press.
(DOI will not work until issue is live.) DOI: http://dx.doi.org/10.2138/am-2017-5830

Fig 1b

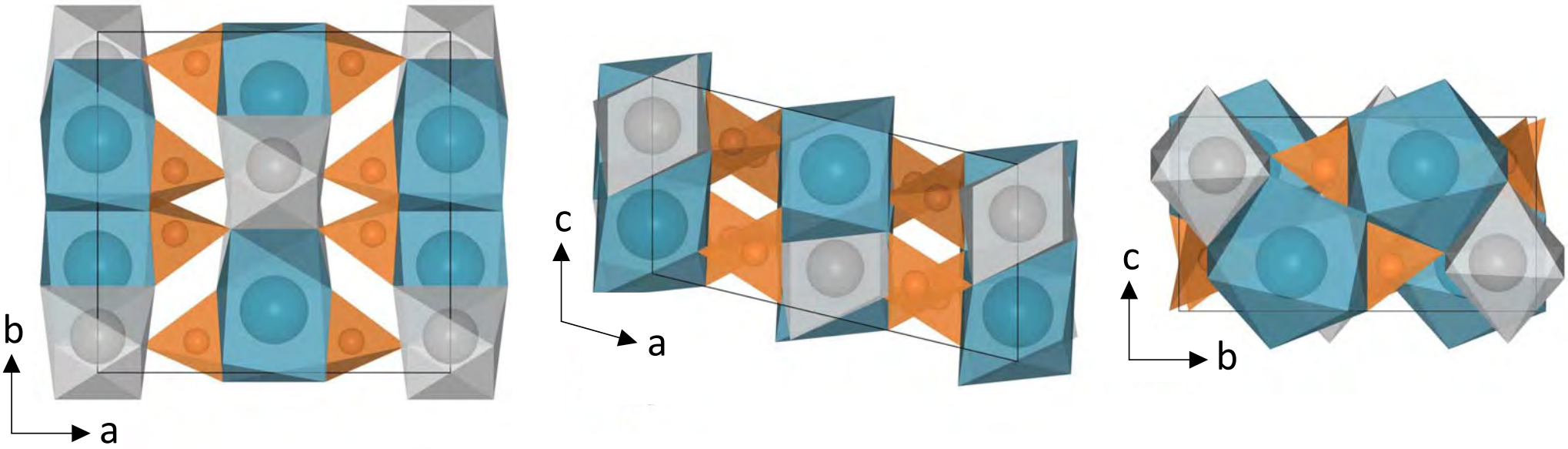

This is a preprint, the final version is subject to change, of the American Mineralogist (MSA)
Cite as Authors (Year) Title. American Mineralogist, in press.
(DOI will not work until issue is live.) DOI: http://dx.doi.org/10.2138/am-2017-5830

Fig 1c

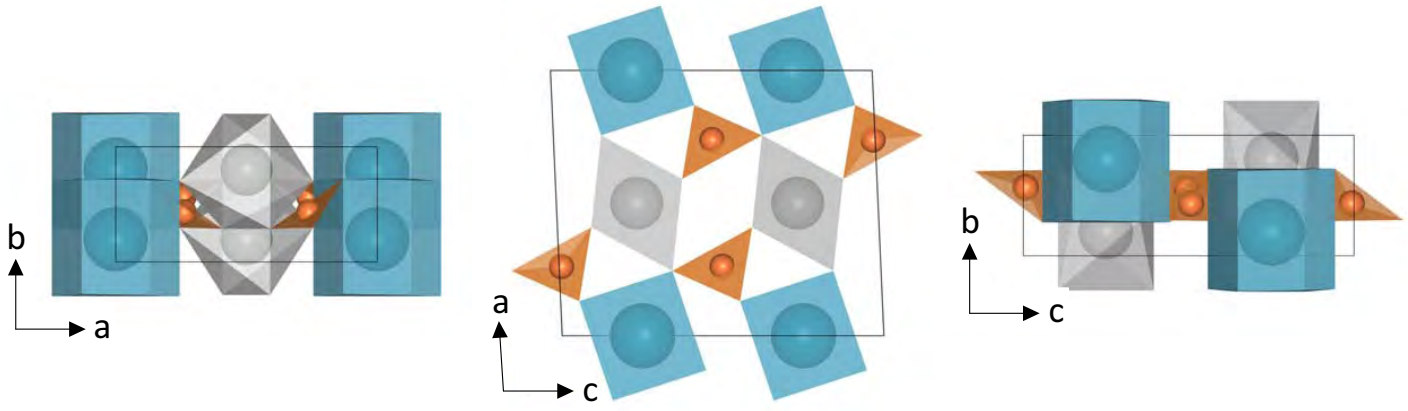

This is a preprint, the final version is subject to change, of the American Mineralogist (MSA)
Cite as Authors (Year) Title. American Mineralogist, in press.
(DOI will not work until issue is live.) DOI: http://dx.doi.org/10.2138/am-2017-5830

Fig 2

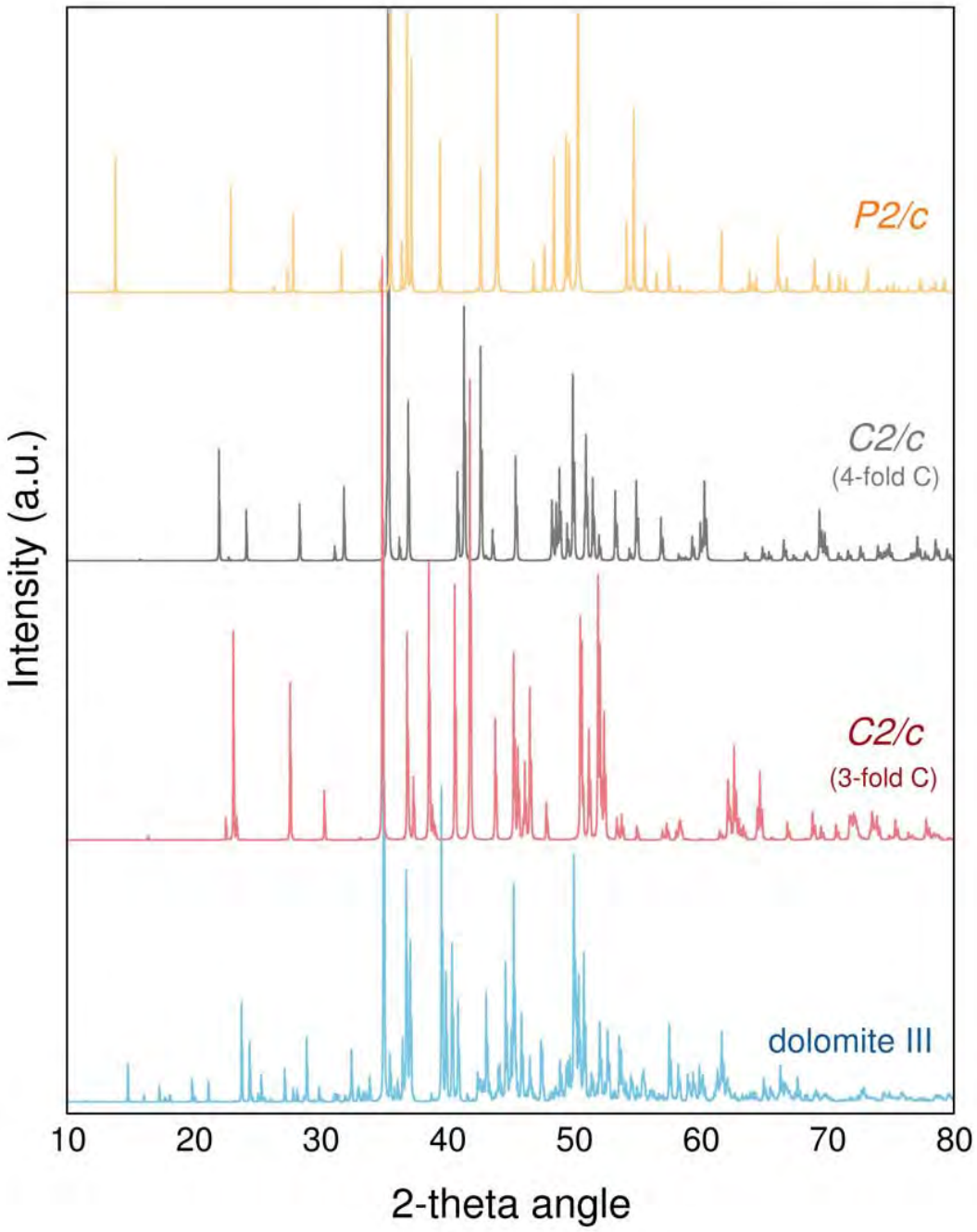

This is a preprint, the final version is subject to change, of the American Mineralogist (MSA)
Cite as Authors (Year) Title. American Mineralogist, in press.
(DOI will not work until issue is live.) DOI: http://dx.doi.org/10.2138/am-2017-5830

Fig 3

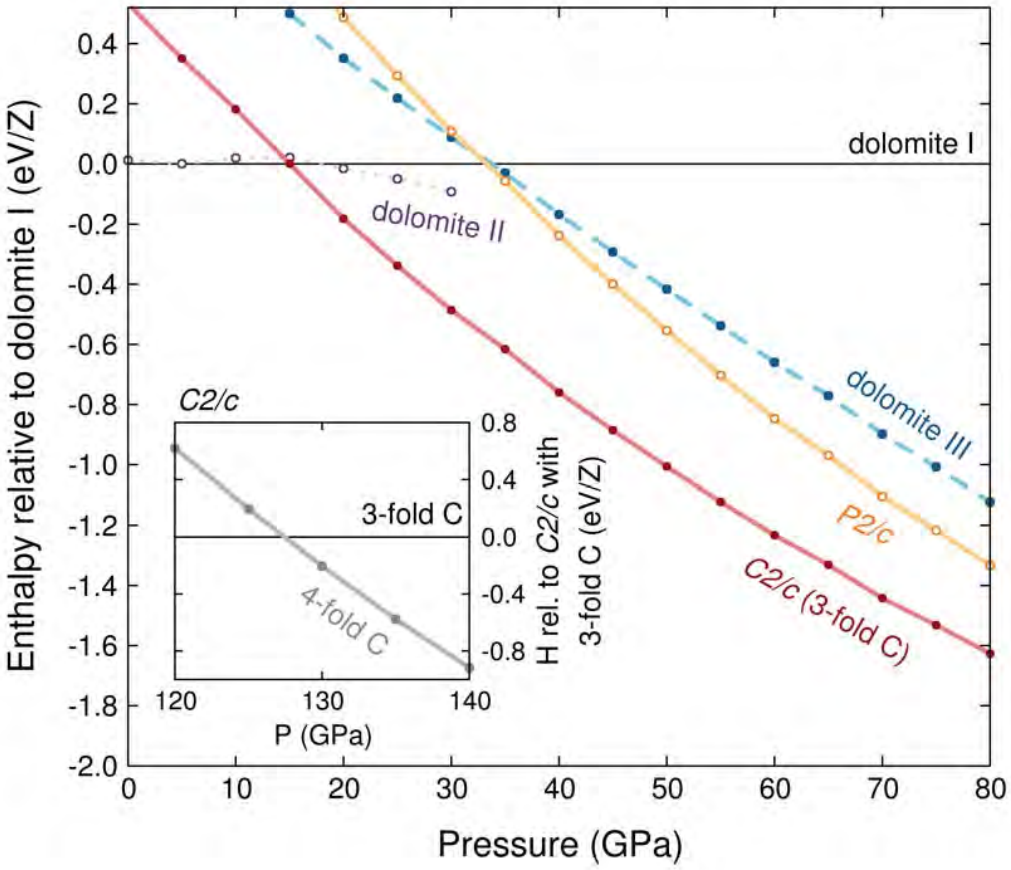

This is a preprint, the final version is subject to change, of the American Mineralogist (MSA)
Cite as Authors (Year) Title. American Mineralogist, in press.
(DOI will not work until issue is live.) DOI: http://dx.doi.org/10.2138/am-2017-5830

Fig 4

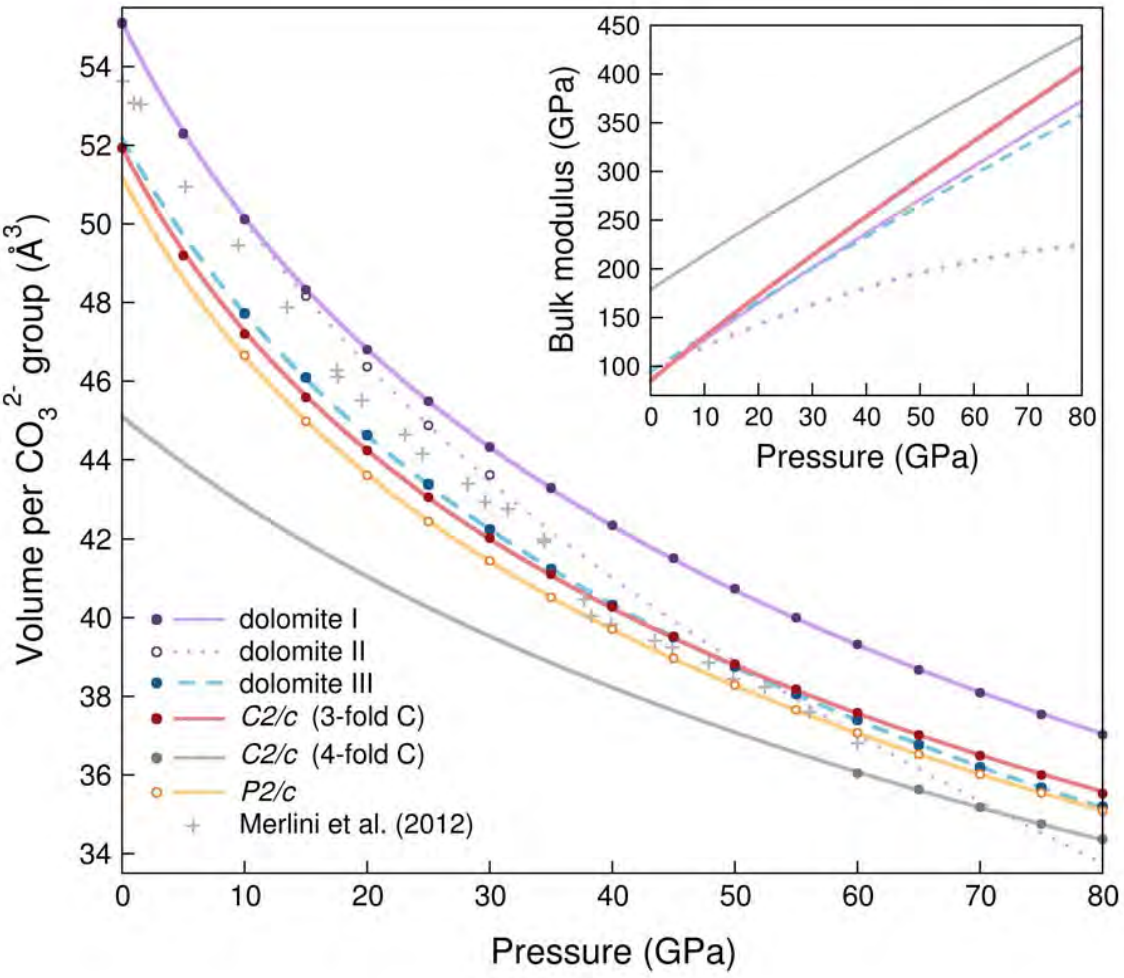

This is a preprint, the final version is subject to change, of the American Mineralogist (MSA)
Cite as Authors (Year) Title. American Mineralogist, in press.
(DOI will not work until issue is live.) DOI: http://dx.doi.org/10.2138/am-2017-5830

Fig 5